3D Processing of Gokturk-2 Imagery

Sultan Kocaman[1], Serkan Ural[1], Gizem Karakas[1], Sedat Bakici[2]
[1] Hacettepe University, Dept. of Geomatics Engineering, 06800 Ankara, Turkey
sultankocaman@hacettepe.edu.tr, ural@hacettepe.edu.tr, gizem.karakas@hacettepe.edu.tr
[2] General Directorate of Land Registry and Cadastre, 06450 Ankara, Turkey
sbakici@tkgm.gov.tr

KEY WORDS: Gokturk-2, satellite imagery, radiometry, geometry, digital surface models

ABSTRACT: Gokturk-2 is the third Earth Observation (EO) satellite of Turkey. It was launched in 2012 and operates at its orbit of 685 km altitude from earth. It has a pushbroom scanner which acquires images from panchromatic (2.5 m), RGB (5 m) and near infrared (5 m) bands. Gokturk-2 also has along-track stereo imaging capability with the angles of ± 30°. Research and validation activities on Gokturk-2 images are so far somewhat limited in the literature. This study aims at validating Gokturk-2 stereo panchromatic (pan) images acquired in March 2015 and May 2017 over Bergama region near Izmir Province of Turkey. The validation mainly focuses on 3D point positioning accuracy and Digital Surface Model (DSM) generation potential from stereo pan images. The image orientation accuracy obtained using ground control points (gcp) and trajectory modelling using higher order polynomials is around 4 pixels for the 2015 stereopair and 2 pixels for the 2017 stereopair. Radiometric quality analysis has been performed prior to DSM generation. The DSMs generated from 2015 and 2017 images have been compared with reference airborne LiDAR data acquired in 2015 with a Riegl sensor. In addition, ground control objects extracted from the aerial images with 30 cm resolution, which were taken and processed by the Turkish General Directorate of Land Registry and Cadastre, have been used as supplementary information for the georeferencing of 2017 images. The results show that despite the accuracy problems in image orientation, DSMs can be generated with sufficient quality.

1. INTRODUCTION

The Gokturk-2 satellite was launched from the Jiuquan Base in China on December 18, 2012 and operates at the nominal altitude of 685 km. It can provide both mono and stereo images in panchromatic and multispectral bands. The ground sample distance (GSD) of the panchromatic imagery is 2.5 meters and a single image strip covers a 5 km x 20 km area. The literature on the investigations of the geometric calibration and validation of the Gokturk-2 images is found to be limited so far. Kupcu et al. (2014) have analyzed the quality of orthoimages obtained by the processing of Gokturk-2 satellite images. The results have shown that a planimetric accuracy of 5 pixels (RMSE) could be achieved from the comparison of 50 reference points. Topan et al. (2016) reported ca. 3 pixels georeferencing accuracy over Zonguldak Testfield using stereo Gokturk-2 images and a total of 72 GCPs. Mutluoglu and Guven (2017) have reported ca. 4 pixels planimetric and 3.5 pixels height accuracy over Konya Testfield using 30 GCPs and 61 independent check points. They have also evaluated the output DSM using 481 reference height points. The mean height error for the study area was found as 9.3 m, which is in accordance to the georeferencing error as well.

The main aim of this study is to contribute to the research activities on the analysis the 3D processing and DSM generation potential of stereo Gokturk-2 images. Two panchromatic stereopairs acquired over Bergama Testfield in 2015 and 2017 have been processed for this purpose. Image orientation has been performed via polynomial modelling of the trajectory data using 40 and 91 ground control points (GCPs) for 2015 and 2017 images, respectively. 2-4 pixels georeferencing accuracy have been achieved during the tests. These values are inferior to the accuracy results reported for SPOT-5, Cartosat-1, ALOS/PRISM, ZY-3, which have a similar GSD to Gokturk-2. Studies show that sub-pixel georeferencing accuracy can be also achieved with an appropriate sensor and trajectory model, accurate camera calibration data, or self-calibration, and well-defined GCPs (Kocaman and Gruen, 2008; Kocaman et al. 2008; Baltsavias et al. 2008; Saunier et al. 2010).

Prior to the DSM generation, image quality has been analyzed in terms of noise, MTF and image histogram statistics. ERDAS Imagine Photogrammetry Tool (Hexagon Geospatial, 2017) has been employed for image orientation and DSM generation. The output DSMs have been compared with reference DSM obtained from airborne LiDAR data over the testfield. The results have been presented and analyzed in the following sections.

2. SENSOR AND DATA CHARACTERISTICS

The imaging sensor on the Gokturk-2 satellite works with the pushbroom principle and can acquire along track stereo images as well (Cinar, 2014; Atak et al., 2015). Gokturk-2 satellite operates at a near polar, sun synchronous

orbit with a revisit time of 2-3 days. Technical specifications of Gokturk-2 sensor is given in Table 1. The processing levels of Gokturk-2 imagery have been defined as (Atak et al., 2015):

- L0: Raw imagery
- L1: Radiometrically corrected
- L1R: Radiometrically corrected and band-to-band registration is completed
- L2: Radiometrically corrected and rectified imagery
- L3: Orthorectified imagery

Table 1. Technical specifications of Gokturk-2 sensor (Cinar, 2014; Atak et al., 2015).

Orbit	Near polar, sun synchronous
Altitude	~685 km
Revisit time	2-3 days
Sensor type	Optical pushbroom imager
Spatial resolution	PAN 2,5 m - MS 5 m
Spectral resolution	PAN : 0,42-0,75 µm Blue: 0,422-0,512 µm Green: 0,5-0,584 µm Red : 0,596-0,75 µm NIR : 0,762-0,894 µm SWIR: 0,8-1,7 µm
Radiometric resolution	11 bit

The Gokturk-2 data processed in this study have been acquired over Bergama Testfield near Izmir, Turkey. We have received 93 GPS surveyed GCPs and airborne LiDAR data from the General Command of Mapping (GCM), Turkey. Gokturk-2 stereo images acquired in May 2015 and March 2017 have been provided by the Turkish Air Force and post processed by TUBITAK Space Technologies Research Institute. Pan, RGB and NIR channel images have been delivered for both acquisitions. Digital terrain model (DTM) and reference vector data had been generated by the Turkish General Directorate of Land Registry and Cadastre, Department of Mapping, using digital aerial photos with 30 cm resolution. The data are described in detail in the following sub-sections.

2.1 Gokturk-2 Imagery

Two stereo Gokturk-2 images have been acquired over Bergama Testfield in 2015 and 2017. Detailed information on the images is given in Table 2. Overviews of both imagery are provided in Figures 1 and 2. The GCP distributions used for the image orientation are provided in Figure 3.

Table 2. Characteristics of Gokturk-2 Bergama images acquired in 2015 and 2017.

Parameter	2015 stereopair	2017 stereopair
Date	22 May 2015	2 March 2017
Sun azimuth	122,393835°	120,133774°
Sun elevation	60,803942°	57,002221°
Stereo angle	+29.9973, -29.9999	29.00, -30.00
Total no. of measured GCPs	91	40

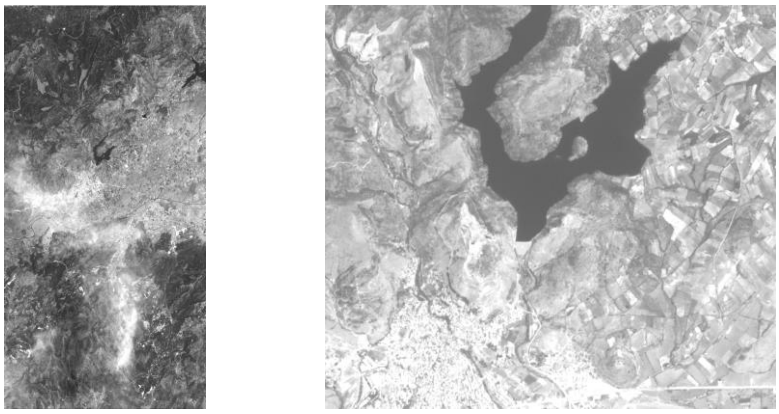

Figure 1. Gokturk-2 image acquired over Bergama Testfield in 2015 (left) and a detailed view of the panchromatic channel image (right).

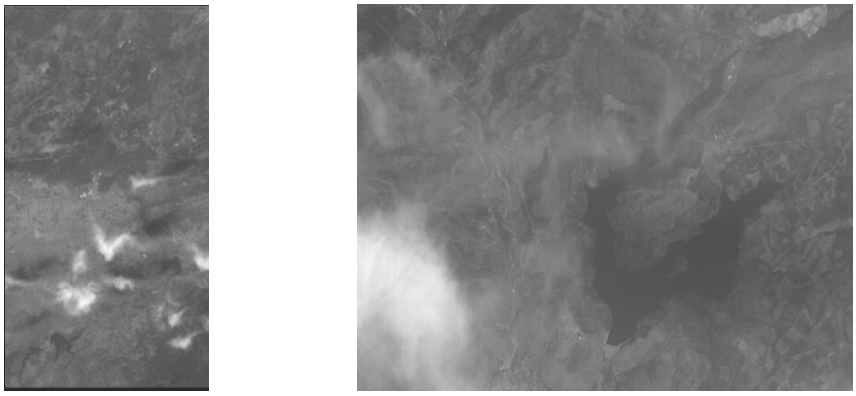

Figure 2. Gokturk-2 image acquired over Bergama Testfield in 2017 (left) and a detailed view of the panchromatic channel image (right).

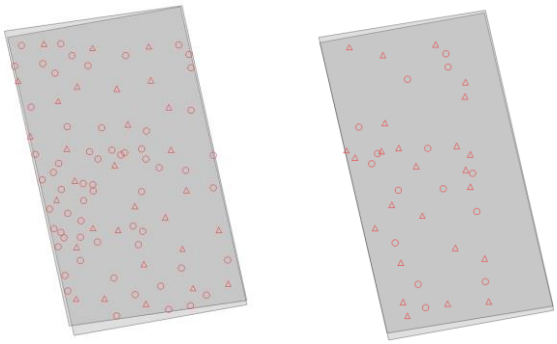

Figure 3. GCP distribution on 2015 (left) and 2017 (right) Gokturk-2 Bergama images. The red triangles and circles denote the control and check points used in orientation, respectively. The grey rectangles denote the coverage areas of the two Gokturk-2 stereopairs.

2.2 Reference LiDAR Data

The LiDAR data over Bergama Testfield have been acquired in 2015. The acquisition has been ordered by a consortium of mapping agencies in Turkey to analyze the suitability of LiDAR data for mapping purposes. Two LiDAR sensors (Optech and Riegl) have been used during the flights performed at two different altitudes (1200 m and 2600 m). Figure 4 shows a part of the DSM obtained from Riegl sensor together with the intensity image.

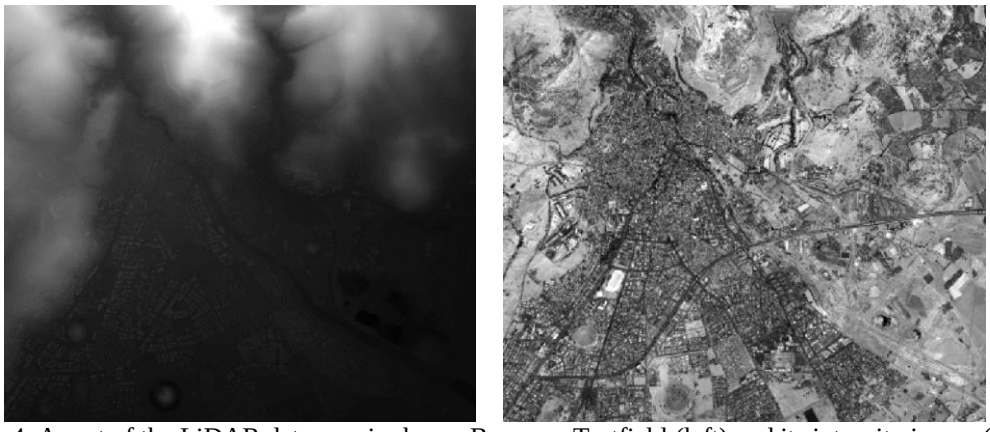

Figure 4. A part of the LiDAR data acquired over Bergama Testfield (left) and its intensity image (right).

3. PROCESSING & ANALYSIS

3.1 Image Quality Analysis

In terms of radiometric quality control, modulation transfer function (MTF) analysis, histogram checks, visual checks and noise analysis on homogeneous surfaces have been performed on both stereopairs. For the noise analysis, image patches selected on one lake surface have been analyzed in terms of mean and standard deviation values. Pan images of all levels (L0, L1, L1R) for 2017 stereo images and L1 and L1R images of 2015 stereopair

have been analysed by this method, which has been proposed by Baltsavias et al. (2001). Image patches selected on the lake surface have been analyses using a window size of 5x5 pixels with a step size of one pixel. Two examples for the selected lake surfaces are given in Figure 5. Only 70% of the results for each patch has been used for the final analysis. The remaining 30% with the largest standard deviations have been excluded from the analysis. Comparing the mean standard deviation results (Table 3) between the L0, L1 and L1R images, the results have been found partially inconsistent and can be even worse in the higher level (radiometrically corrected) images.

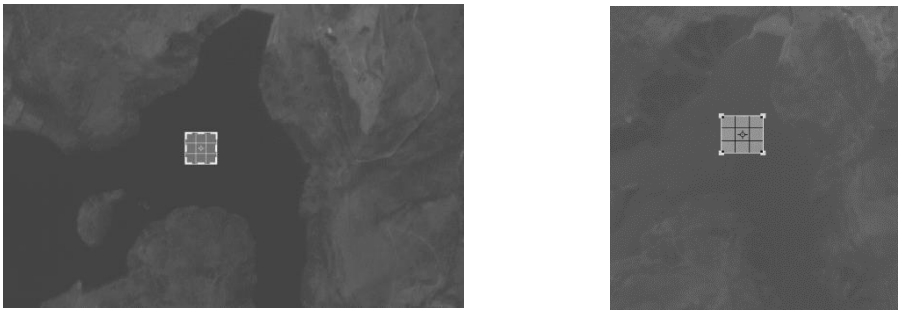

Figure 5. Two of the lakes with Gokturk-2 L1R image patches (left: 2015 right:2017)

Table 3. Image noise analysis results

Image	Gokturk-2 2015						Gokturk-2 2017					
	Part1			Part2			Part1			Part2		
Level	L0	L1	L1R	L0	L1	L1R	L0	L1	L1R	L0	L1	L1R
Min. Std. Dev.	N.A.*	0.6	0.6	N.A.	0.6	0.6	0.6	0.6	0.6	0.6	0.6	0.6
Max. Std. Dev.	N.A.	29.4	29.4	N.A.	26.2	39.1	20.4	0.9	30.2	20.3	32.4	32.3
Mean Std. Dev.	N.A.	17,2	17,2	N.A.	14,9	22,8	11,9	0,01	17,7	11,9	19,1	19,9

**N.A.: Not available*

The MTF is a fundamental criterion for measuring the spatial resolution performance of the imagery and is mathematically defined as the normalized magnitude of the Fourier transform of the point spread function (PSF) or line spread function (LSF) of an imaging system (Akca and Gruen, 2009). The Gokturk-2 pan images have been analyzed in terms of MTF, ESF and LSF using Quick MTF software (2017). The software provides spatial frequency by the contrast 0.5 (50% of MTF) and this value is called MTF50. Road edges both along the flight path and also perpendicular to the flight path have been selected for the MTF analysis as proposed by Crespi and de Vendictis (2009). Several road lines in along-track and across-track directions have been analyzed. Examples of the line patches are given in Figure 6. The MTF results in Table 4 are statistical summaries of all samples per image and direction (i.e. along-track and across-track). According to Quick MTF (2017), a larger MTF50 value yield to a better spatial resolution. It can be said that the along-track samples indicate higher resolution for both datasets. In addition, the 2015 images have superior spatial resolution in both directions.

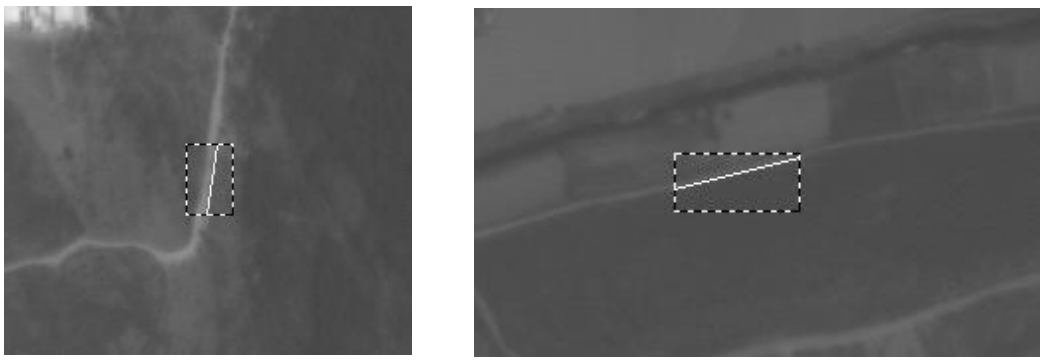

Figure 6. Examples to the along-track (left) and across-track (right) lines used for the MTF analysis.

The histogram statistics for 2015 L1R part 1 image have shown that the average intensity value is 253 with a standard deviation of 52 pixels. The histogram contains a total of 752 different intensity values. In the 2017 L1R part 1 image, the histogram contains 384 different values distributed throughout the histogram (0 to 65535). The average intensity value is 23560 with a standard deviation of 5682 pixels. This problem should be investigated in detail in the future. Both histograms indicate a dynamic range of 9-10 bits. This phenomenon has been checked with other pan image levels (L0 and L1) and confirmed.

Table 4. MTF50 results of both panchromatic images.

	Gokturk-2 2015		Gokturk-2 2017	
Parameter	Along-track (5 Samples)	Across-track (5 Samples)	Along-track (5 Samples)	Across-track (5 Samples)
Mean	0.55 c/p	0.29 c/p	0.32 c/p	0.25 c/p
Std. Deviation	0.24 c/p	0.17 c/p	0.06 c/p	0.03 c/p
Min.	0.33 c/p	0.02 c/p	0.24 c/p	0.22 c/p
Max.	0.99 c/p	0.48 c/p	0.42 c/p	0.29 c/p

3.2 Gokturk-2 Image Orientation

The L1R images have been oriented using the generic polynomial model in ERDAS Imagine Photogrammetry. Initial image rotations have been provided in the support files of the images. The camera constant and CCD pixel size parameters have been provided by the Turkish Air Force. Large numbers of GCPs have been used for the orientation of both stereopairs due to the lack of image trajectory data and adequate sensor calibration. A total of 94 GCPs were provided by GCM. 91 points could be measured in the 2015 images. For image orientation, 30 of those were used as control and the remaining 61 were used as reference check points. Regarding the 2017 images, only 33 of the provided points could be measured. In order to ensure a suitable GCP distribution, 7 more points have been extracted from road vector intersections provided by the Turkish General Directorate of Land Registry and Cadastre and measured in the images. During image orientation, 25 points were used as control and 15 points were used as check points. Mainly road intersections were used as ground control points. The GCP and check point distributions are shown in Figure 3. The image measurement accuracy of the control points can be assumed as 0.5 pixel due to poor definition of the points. One example to the measured GCPs is given in Figure 7.

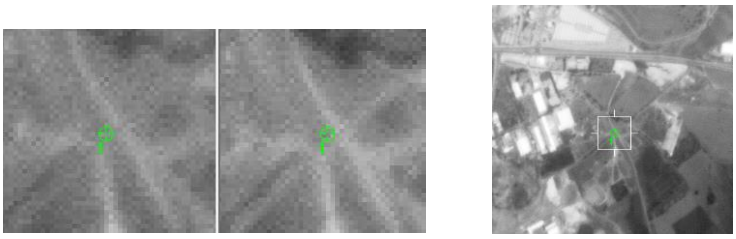

Figure 7. Image definition of one GCP in 2015 stereopair.

The image orientation have been performed using polynomial modeling of the exterior orientation parameters. After running several tests with different orders of polynomial functions, the results which led to the highest absolute accuracy based on the check point residuals are presented here. Regarding the 2015 stereopair, first order polynomials for X,Y and the rotation angles, and a constant translation parameter for the height (a total of 11 parameters) have been selected. However, the triangulation report indicated that 3rd degree polynomial parameters for X and Y, and first order polynomial parameters for Z and the angles have been estimated by the software. This setting has led to over-parameterization in the adjustment, which can be observed in the extremely low sigma naught value (Table 5). The 2017 stereopair has been oriented with first order polynomial parameters for X,Y,Z, Omega and Kappa, where Phi is modeled the best using a second order parameter. The $Image_x$ and $Image_y$ parameters in Table 5 correspond to the image residuals of the control points. $RMSE_{X,Y,Z}$ values have been obtained from the comparison of the given coordinates of the check points with the computed coordinates after the adjustment. The triangulation accuracy of the 2017 stereopair has been found to be superior.

Table 5. Georeferencing accuracies obtained from generic polynomial models for 2015 and 2017 stereopair.

	Sigma naught	$Image_x$	$Image_y$	$RMSE_X$	$RMSE_Y$	$RMSE_{XY}$	$RMSE_Z$
Gokturk-2 2015	0.02 pixel	3.4 pixel	3.3 pixel	11.9 m	10.3 m	11.1 m	6.9 m
Gokturk-2 2017	0.21 pixel	3.8 pixel	2.6 pixel	6.0 m	5.2 m	5.6 m	4.7 m

3.3 DSM Generation and Comparison

Since the 2017 stereopair suffer from clouds, the DSM generation is performed in selected parts of the L1R images. The DSMs have been generated using the eATE module of ERDAS Imagine Photogrammetry software. The tool uses normalized cross correlation (NCC) for image matching (ERDAS Imagine Help). A window size of 9x9 pixels has been selected for matching of both stereopairs. A DSM for the whole image has been generated for the 2015 image. For the 2017 image, five sub-areas have been selected with different land cover, land use and topography characteristics. The five sub areas selected on the 2017 image and an overlay of the LiDAR data over the 2017 images are given in Figure 8. The resulting DSMs have been compared with the LiDAR DSM generated

from Riegl data. For the comparison, CloudCompare tool, which is an open source software (http://www.danielgm.net/cc/), has been used. CloudCompare employs the Iterative Closest Point (ICP) method proposed by Besl and McKay (1992), which has been used for initial co-registration of the two point sets (CloudCompare, 2017). Three translation parameters have been estimated between each point cloud pair, except the 2015 data, before the comparison. The residuals after the translation removal were analyzed here. For the 2015 datasets, a direct comparison without translation removal had be carried out due to an unknown issue with the software. The comparison results are provided in Table 6. The Shift X, Shift Y and Shift Z values denote the translation parameters computed by ICP method. The Euclidian and $\sigma_{Euclidian}$ parameters denote the mean Euclidian distance calculated from all residuals and the corresponding standard deviation, respectively. Figures 9-20 show the original point sets used for the comparisons and the residuals provided by the tool.

Overall results given in Table 6 show that residual errors are around half of the GSD in all comparisons of the 2017 data. Minor differences are mainly due to different topography, land cover type and different numbers of points being compared in each set. Dense point matching procedure has returned more successful matches in urban areas, where the images have more contrast and texture (Figures 11 and 12). The number of successfully matched points are especially low in hilly areas, where there is less settlement. Another reason for lack of matches in hilly areas can be large stereo angles (± 30º). The larger errors in 2015 results comprise the georeferencing errors as well.

Table 6. LiDAR DSM comparison results for both 2015 and 2017 imagery.

	Shift X (m)	Shift Y (m)	Shift Z (m)	Euclidian (m)	$\sigma_{Euclidian}$ (m)
Gokturk-2 2017- Sub area 1	1.0	1.7	-7.9	1.3	1.2
Gokturk-2 2017- Sub area 2	0.1	-2.7	-3.5	-1.3	1.5
Gokturk-2 2017- Sub area 3	-0.8	-1.3	-7.6	1.2	1.5
Gokturk-2 2017- Sub area 4	-5.6	1.2	-5.5	1.1	1.4
Gokturk-2 2017- Sub area 5	-4.3	0.5	3.3	1.2	1.2
Gokturk-2 2015	N.A.	N.A.	N.A.	4.6	3.7

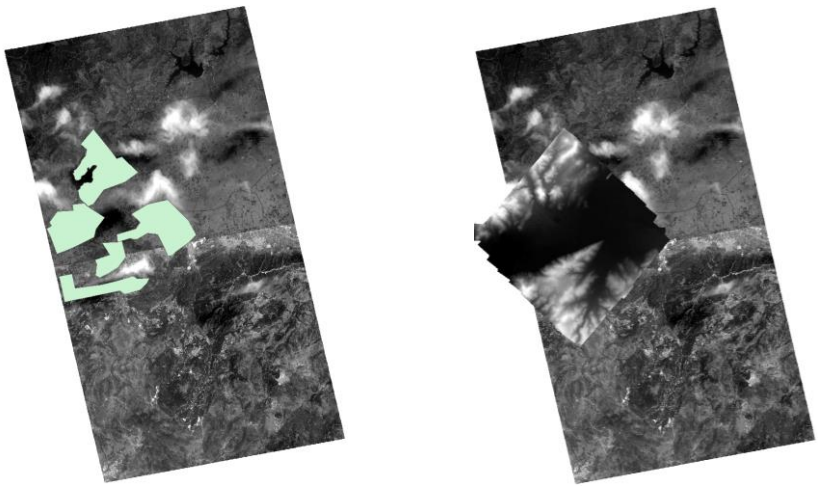

Figure 8. Five sub areas selected for DSM generation in 2017 images and overlay of the LiDAR data (right).

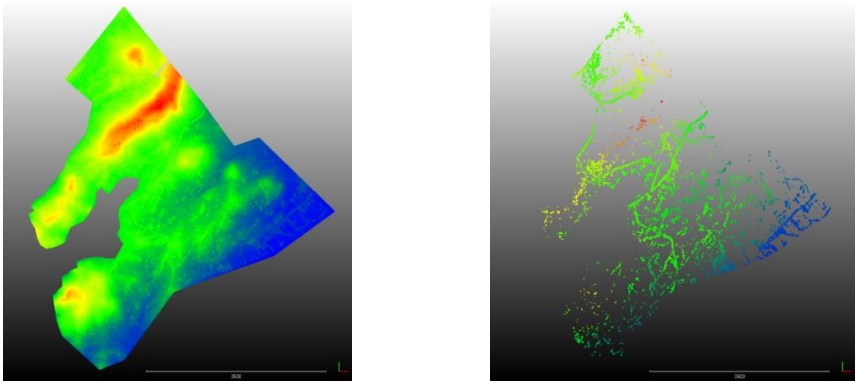

Figure 9. The LiDAR DSM (left) and the Gokturk-2 2017 DSM (right) in sub-area 1. The ICP translation results are 1.0, 1.7 and -7.9 meters in X,Y, and Z, respectively.

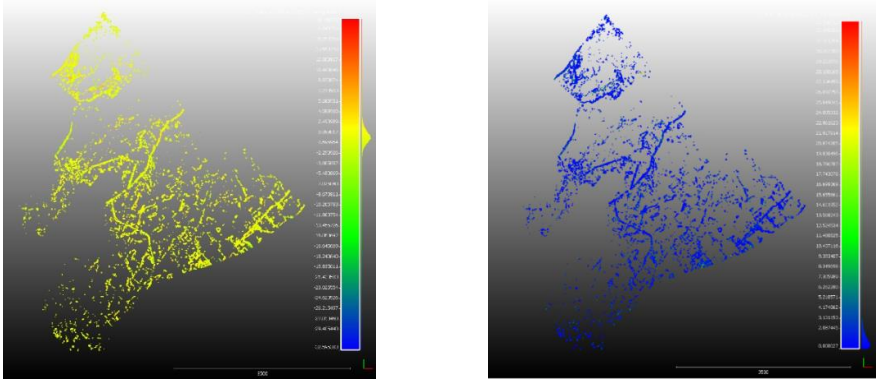

Figure 10. The residuals in Z (left) and the Euclidian distance (right) for the sub-area 1. The mean Euclidian distance error in and the standard deviation are 1.3 and 1.2 meters, respectively.

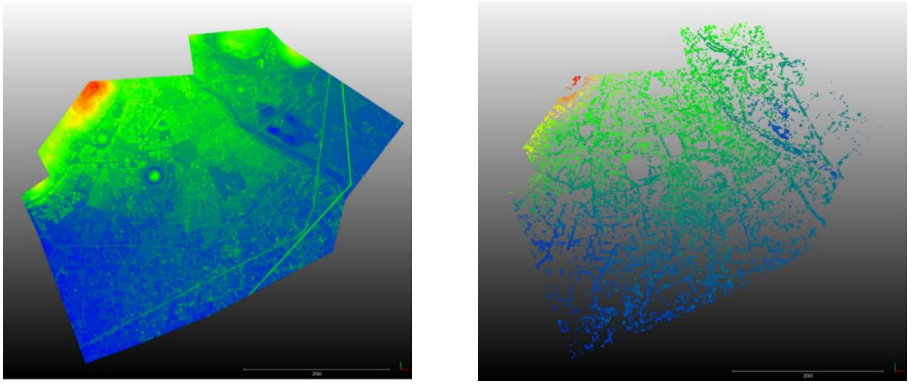

Figure 11. The LiDAR DSM (left) and the Gokturk-2 2017 DSM (right) in sub-area 2. The ICP translation results are 0.1, -2.7 and -3.5 meters in X,Y, and Z, respectively.

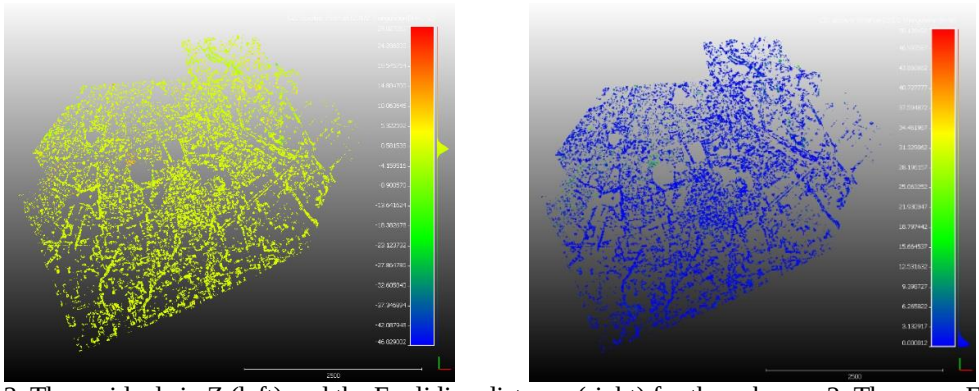

Figure 12. The residuals in Z (left) and the Euclidian distance (right) for the sub-area 2. The mean Euclidian distance error in and the standard deviation are -1.3 and 1.5 meters, respectively.

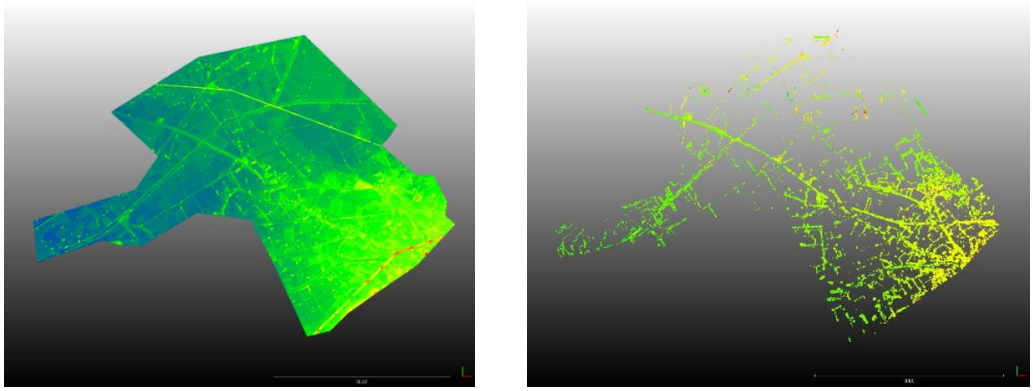

Figure 13. The LiDAR DSM (left) and the Gokturk-2 2017 DSM(right) in sub-area 3. The ICP translation results are -0.8, -1.3 and -7.6 meters in X,Y, and Z, respectively.

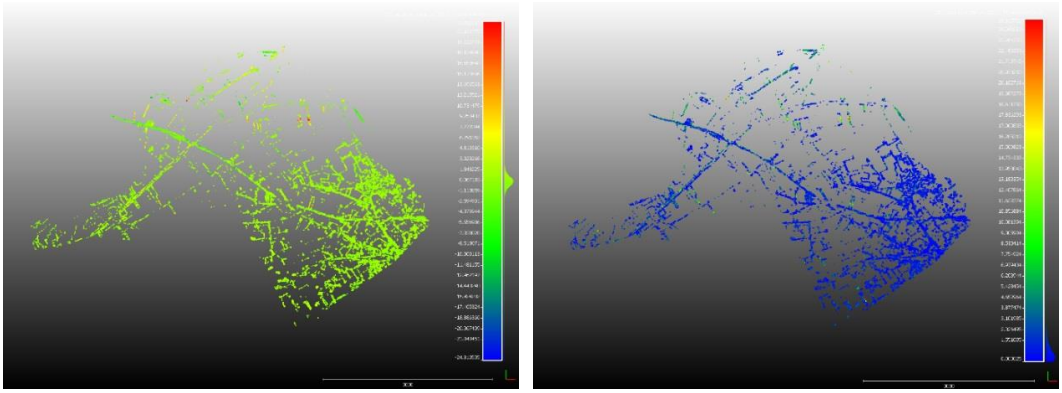

Figure 14. The residuals in Z (left) and the Euclidian distance (right) for the sub-area 3. The mean Euclidian distance error in and the standard deviation are 1.2 and 1.5 meters, respectively.

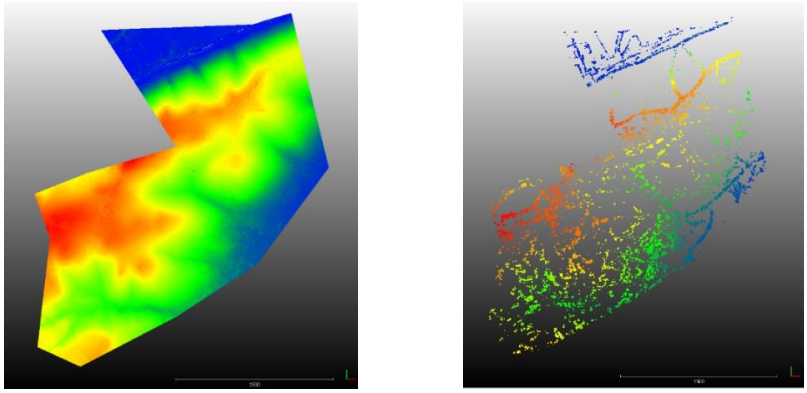

Figure 15. The LiDAR DSM (left) and the Gokturk-2 2017 DSM (right) in sub-area 4. The ICP translation results are -5.6, 1.2 and -5.5 meters in X,Y, and Z, respectively.

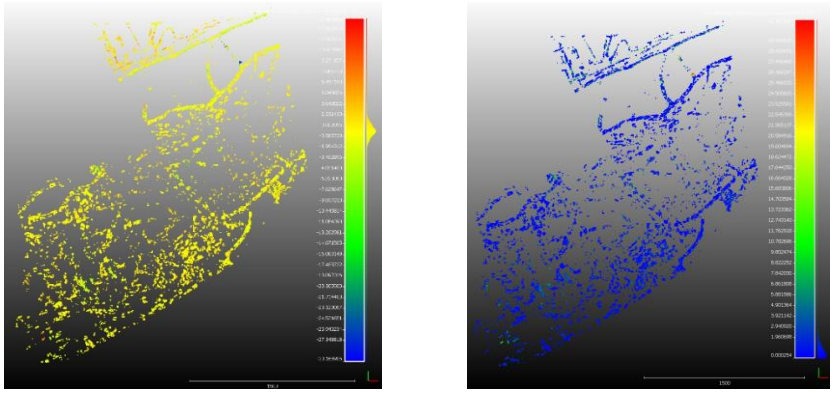

Figure 16. The residuals in Z (left) and the Euclidian distance (right) for the sub-area 4. The mean Euclidian distance error in and the standard deviation are 1.1 and 1.4 meters, respectively.

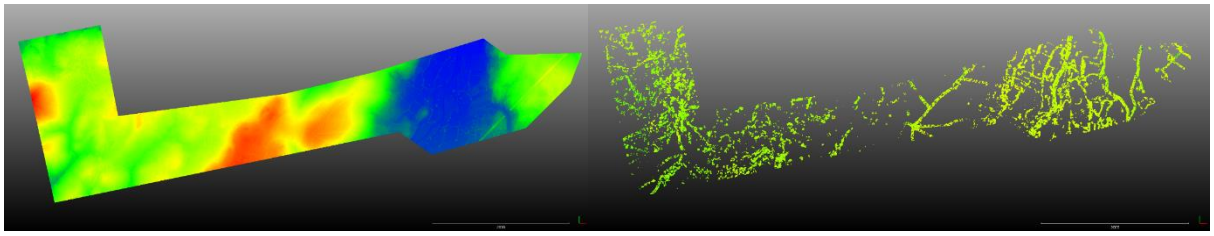

Figure 17. The LiDAR DSM (left) and the Gokturk-2 2017 DSM (right) in sub-area 5. The ICP translation results are -4.3, 0.5 and 3.3 meters in X,Y, and Z, respectively.

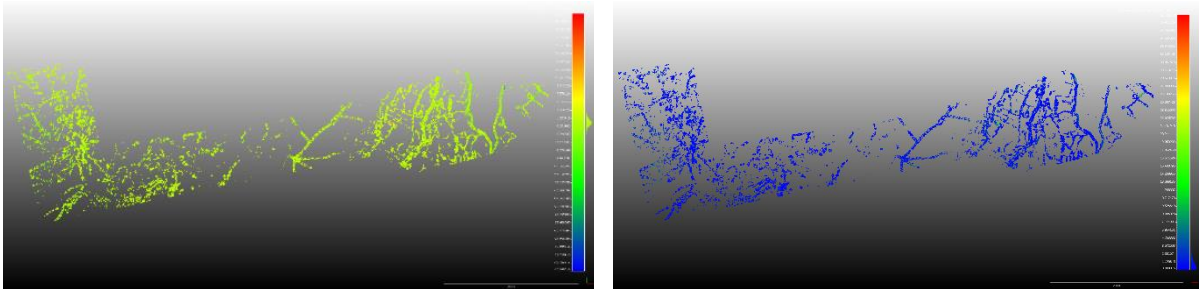

Figure 18. The residuals in Z (left) and the Euclidian distance (right) for the sub-area 5. The mean Euclidian distance error in and the standard deviation are both 1.2 meters.

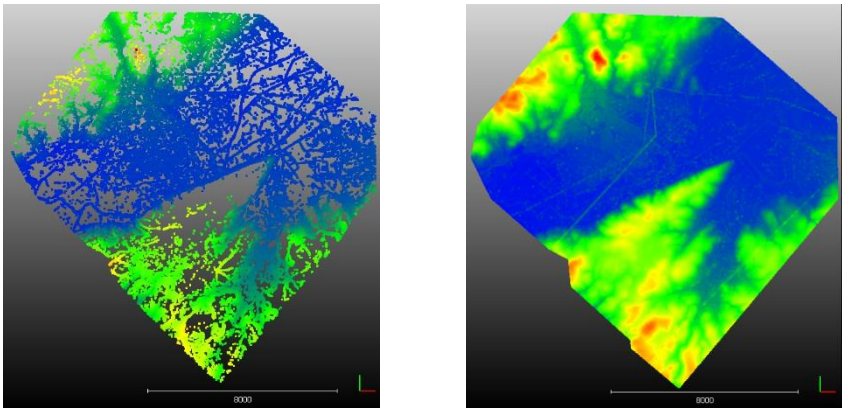

Figure 19. The LiDAR DSM (left) and the Gokturk-2 2015 DSM (right). ICP translation could not be performed for this dataset.

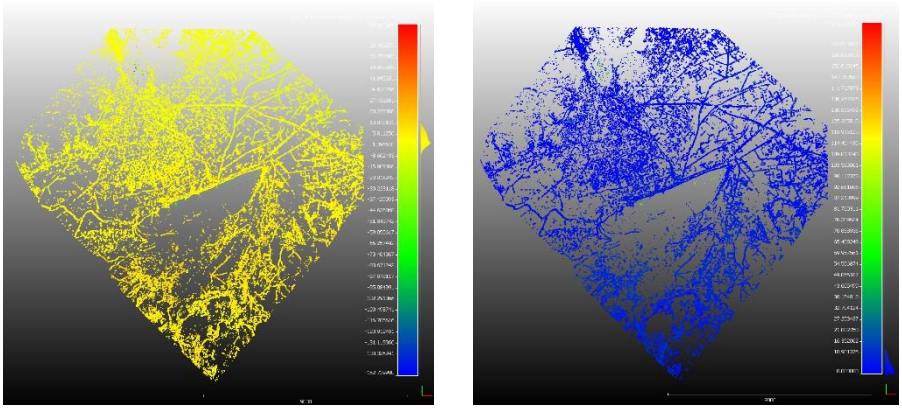

Figure 20. The residuals in Z (left) and the Euclidian distance (right) for Gokturk-2 2015 DSM. The mean Euclidian distance error in and the standard deviation are 4.6 and 3.7 meters, respectively.

4. CONCLUSIONS

The main aim of this study is to analyze the 3D processing and automatic DSM generation capability of Gokturk-2 stereo imagery. Images acquired over Bergama Testfield in 2015 and 2017 have been used for this purpose. Initially, the image quality, which is crucial for successful image matching, has been assessed by using histogram, noise and MTF analyses as well as visual checks. A number of ground surveyed GCPs and reference vector data have been used for image orientation. For the assessment of DSM quality, airborne LiDAR data have been used as reference.

Unfortunately, the direct georeferencing accuracy could not be assessed due to the lack of image trajectory and accurate camera calibration data. The image orientation accuracy obtained from 61 independent check points for 2015 stereopair is 4.4 pixels (11.1m) in planimetry and 2.8 pixels (6.9 m) in height. For the 2017 stereopair, the planimetric accuracy is 2.2 pixels (5.6 m) in planimetry and 1.9 pixels (4.7 m) in height. These results have been obtained from polynomial modeling of the image trajectory using large numbers of control points. Only the focal length and the CCD pixel size parameters exist for the interior orientation, which have not been calibrated recently. Improvements to the image trajectory data and the camera calibration would most likely increase the geometric accuracy of the sensor even when using a small number of GCPs.

The DSM comparison results show that they can be generated with sufficient accuracy from Gokturk-2 stereo images. After removal of the constant shifts (translations in three directions), ca. 0.5 pixel mean error remains in the height residuals. The main error source for the DSMs is the poor image orientation. On the other hand, inferior radiometric quality of the images causes issues in the completeness of the DSMs. Different types of artefacts (e.g. jpeg compression and stripes), high noise level in L1R images and poor texture in the images cause unsuccessful matches. Radiometric improvements would increase the number of matched points, which would lead to more complete DSMs.

ACKNOWLEDGEMENTS

The authors are thankful to the Image Processing Group at the TUBITAK Space Technologies Research Institute for their open communication. Additional thanks go to the General Command of Mapping and the Turkish Air Force for provision of the GCPs and images. The authors express out appreciation to the staff members of the Turkish General Directorate of Land Registry and Cadastre, Department of Mapping for their support.

REFERENCES

Akca, D., Gruen, A., 2009. "Comparative Geometric and Radiometric Evaluation of Mobile Phone and Still Video Cameras". The Photogrammetric Record 24(127), pp. 217–245.

Atak, O., Erdoğan, M., Yılmaz, A., 2015. Göktürk-2 Uydu Görüntü Testleri. Harita Dergisi, January, Vol. 153.

Baltsavias, E. P., Pateraki, M., Zhang, L., 2001. Radiometric and geometric evaluation of IKONOS Geo images and their use for 3D building modeling. Joint ISPRS Workshop on "High Resolution Mapping from Space 2001, Hannover, Germany, 19-21 September.

Baltsavias E., Kocaman S., Wolff K., 2008. Analysis of Cartosat-1 images regarding image quality, 3D point measurement and DSM generation. The Photogrammetric Record, 23(123), 305-322.

Besl, P.J., and McKay, N.D., 1992. A method for registration of 3D shapes. IEEE Transactions on Pattern Analysis and Machine Intelligence, 14 (2), pp. 239-256.

CloudCompare, 2017. Users Manual 2.1. Retrieved September 27, 2017 from http://www.danielgm.net/cc/doc/qCC/Documentation_CloudCompare_version_2_1_eng.pdf

Cinar, E., 2014. GÖKTÜRK-2 Uydu Sisteminin Operasyonel Kabiliyetleri. Oral presentation at Yer Gözlem Uydu Teknolojileri ve Veri Kıymetlendirme Çalıştayı, 19-20 March, Ankara, Turkey.

Crespi, M., de Vendictis, L., 2009, A Procedure for High Resolution Satellite Imagery Quality Assessment. Sensors, 9, pp. 3289-3313. doi:10.3390/s90503289

Hexagon Geospatial, 2017. ERDAS Imagine. Retrieved September 27, 2017 from http://www.hexagongeospatial.com/products/power-portfolio/erdas-imagine

Kocaman S., Wolff K.,Gruen A., Baltsavias E. 2008. Geometric Validation of Cartosat-1 Imagery. 21st ISPRS Congress, Beijing, China.

Kocaman S., Gruen A., 2008. Orientation and self-calibration of ALOS PRISM imagery. The Photogrammetric Record, 23(123), 323-340.

Kupcu, R., Teke, M., Çabuk, A., 2014. RASAT ve Gokturk-2 Görüntülerinin Ortorektifikasyon Başarimina Referans Ve Sayisal Yükseklik Modeli Seçiminin Etkisi. UZAL-CBS 2014 Symposium. 14-17 October. Istanbul. Retrieved November 27, 2015 from http://www.uzalcbs2014.sempozyumu.net/bildiriler.php.

Mutluoglu, O., Guven, M., 2017. Accuracy Investigation of DEM Based On Göktürk-2 Stereo Images. SUJEST, v.5, n.2, DOI: 10.15317/Scitech.2017.83

Quick MTF, 2017. Retrieved September 24, 2017 from http://www.quickmtf.com

Saunier S., Chander G., Goryl Ph., Santer R., Bouvet M., Collet B., Mambimba A., Kocaman S., 2010. Radiometric, Geometric, and Image Quality Assessment of ALOS AVNIR-2 and PRISM Sensors. IEEE Transactions on Geoscience and Remote Sensing, 48(10), 3855-3866.

Topan, H., Cam, A., Oruç, M., Teke, M. 2016. Göktürk-2 Görüntülerinin Radyometrik ve Geometrik Açıdan Değerlendirilmesi. 6. Uzaktan Algılama-CBS Sempozyumu, Adana, Turkey.